



## Numerical Prediction of Stator Diameter Effect on the Output Torque of Ultrasonic Traveling-wave Motor, using Finite Elements Simulation

H. Rahafrouz<sup>a</sup>, A. Manouchehrifar<sup>a</sup>, F. Haji Aboutalebi<sup>\*b</sup>

<sup>a</sup> Department of Mechanical Engineering, Islamic Azad University of Khomeinishahr, Isfahan, Iran

<sup>b</sup> Department of Mechanical Engineering, University of Isfahan, Isfahan, Iran

### PAPER INFO

#### Paper history:

Received 29 April 2015

Received in revised form 18 November 2015

Accepted 1 May 2016

#### Keywords:

Ultrasonic Traveling-wave Motor

Increasing the Diameter

Output Torque

Rotational Speed

### ABSTRACT

Nowadays, piezoelectric materials have wide applications in various industries. Therefore, investigation of these materials and their applications has a special importance. In this paper first, the natural frequencies of a traveling-wave piezoelectric motor are achieved, using finite elements simulations. Then, applying an alternative electrical voltage to the piezoelectric ring, a traveling wave is generated in the stator, and the stability, damping effects, and characteristics of the traveling wave are studied. Additionally, the output torque and rotational speed of the motor are obtained and validated by experimental values. Finally, the stator diameter is increased and its effects on the output torque and rotational speed are inspected. The results reveal that the output torque and maximum rotational speed of the enlarged motor respectively increases and decreases.

doi: 10.5829/idosi.ije.2016.29.05b.16

## 1. INTRODUCTION

In the recent years, increasing the use of piezoelectric materials in the aerospace, robotics, and different industries is really noticeable. For this purpose, many researchers have focused on these materials and their applications. The piezoelectric traveling-wave motors or ultrasonic motors (USMs) are one of the most well-known actuators and are widely employed in various industries. Some advantages of the USMs are:

- Producing high power at low speed and not needing to any gear.
- Using the friction principle to drive, eliminating the need for a separate break.
- Having vast application in vacuum spaces because of not requiring any lubrication.
- Having the high efficiency near the stall torque, unlike the electromagnetic motors.
- Leading to high-torque density due to the high torque and compact size.

- Not affecting the magnetic field.
- Having silent operation.

On the other hand, some disadvantages of the USMs are:

- Inappropriate for heavy load operation.
- Unsuitable for the heavy continuous and long operations.
- High frequency excitation is required.
- Wear resistant material is needed.

The principle of a USM is generating a travelling wave on the stator through applying alternative voltage to the piezoelectric actuators operating in the ultrasonic range [1]. Every point on the surface of the stator has elliptical motion due to the travelling-wave. The crests of the travelling-waves are in friction contact with the rotor (contact area). Hence, because of the elliptical motion, the energy of the traveling wave is translated to the rotor and makes the rotor spin. Figure 1 shows a USM configuration, based on a contact system compressing rotor and stator. Among the reported researches, several published investigations describe a variety of designs and their operating principles, and characteristics [1-5].

\*Corresponding Author Email: [f.hajiboutalebi@eng.ui.ac.ir](mailto:f.hajiboutalebi@eng.ui.ac.ir) (F. Haji Aboutalebi)

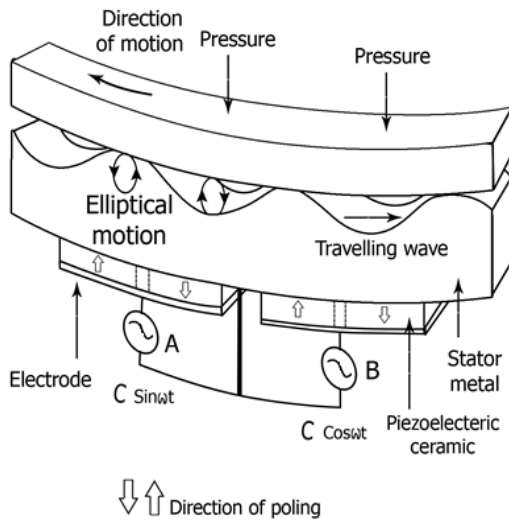


Figure 1. Schematic image of a travelling-wave motor

Recently, various numerical modeling such as Kirchhoff [1], Mindlin plate model combined with elastic foundation or half-space contact model [6-8], equivalent electric circuit [9-11], analytical methods [3, 12], and finite elements methods [13-20] have been developed to model the USMs.

On the other hand, energy method was applied to calculate rotor response with loose rotating disk on it [21]. Rotor flux based MRAS (RF-MRAS) and reactive power based MRAS (RP-MRAS) for rotor resistance estimation was designed and validated by Nandhini Gayathri et al. [22]. Moreover, mechanical response of a piezoelectrically sandwiched nano-beam was studied, employing the nonlocal theory [23]. The static and dynamic stabilities of a parametrically excited torsional microactuator was addressed by Abbasnejad et al. [24].

Because of the accurate modeling of piezoelectric coupled stator, rotor, and contact interface, the finite element method is more accurate than the others. Modeling with the commercial softwares such as ABAQUS is one of the most effective methods, and many attempts have been made to increase the effectiveness of the USMs [16, 18, 20]. In order to obtain a higher output torque, a two-sided USM has been modeled and its output parameters have been compared with one-sided type [13]. In the above mentioned research, it has been shown that a two-sided USM has larger output torque and is more effective in comparison with the one-sided USM. Furthermore, there has been some efforts to obtain the maximum torque through some ways such as optimizing contact area [18] and finding the best wave number [20].

In this paper, the main objective is numerically studying the effect of stator diameter on the output torque, stability, damping effects, and characteristics of the traveling wave in a traveling-wave piezoelectric

motor. For this goal, first of all, a Mock-Shinsei motor is simulated, using the ABAQUS finite element software. Then, the output torque and rotational speed of the motor is obtained and validated by the experimental values. Finally, the effects of increasing stator diameter on the output torque and stresses are investigated.

## 2. DESIGN PARAMETERS OF USM

Diameter of the stator is one of the main parameters in design of the USMs. The maximum achievable stall torque is in direct relation to the cubed diameter (the contact area is directly proportional to the squared diameter). Moreover, the no-load speed is in inverse proportion to the diameter as the following [13]:

$$T_{Stall} \propto D^3 \quad (1)$$

$$\omega_{no-load} \propto D^{-1} \quad (2)$$

where,  $T_{Stall}$ ,  $D$ , and  $\omega_{no-load}$  respectively are the stall torque, diameter, and no-load rotational speed. On the other hand, the stall torque is directly related to the resonance frequency, according to equation [3]:

$$T_{Stall} \propto \omega_f \quad (3)$$

in which,  $\omega_f$  is resonance frequency. Increasing the diameter would directly make the torque squared; however it could disadvantageously result in audible resonance frequency. On the other hand, increasing the vibration mode to maintain resonance frequency in the ultrasonic range would reduce the possibility of the stability.

## 3. NUMERICAL SIMULATIONS OF USM

The stator of Mock-Shinsei motor consists of a rotor and a stator. Figure 2 shows the explosive map of the motor which is modeled in the ABAQUS software. The stator is composed of a substrate and a piezoelectric ring. The substrate ring, the piezoelectric ring and the rotor, correspondingly are made of phosphor bronze, PZT-4, and aluminum.

Furthermore, a contact layer made of Ekonol/PTFE blend is bonded to the rotor which behaves as an interface between the rotor and stator. The material properties of the piezoelectric ring, contact layer, rotor, and substrate are tabulated in Tables 1-4 [13, 18]. A constant force of 160N is applied to the rotor as a preload for pressing the rotor on the substrate and increasing the friction force. For assigning this preload, the RP-1 (reference point) is tied to the inner ring of the rotor and the force is applied to this point, according to Figure 2.

The piezoelectric ring is partitioned into eighteen sectors. Sixteen of the sectors are alternatively poled in different directions, and two of them are set neutral, as Figure 3 reveals. The positive and negative signs show the direction of the poled sectors, while, the sectors with no sign are neutral. Figure 4 shows the polarization of the piezoelectric ring. For this purpose, two local coordinates are defined so that their axes z (or 3) are opposite to each other and parallel to the axis of the ring.

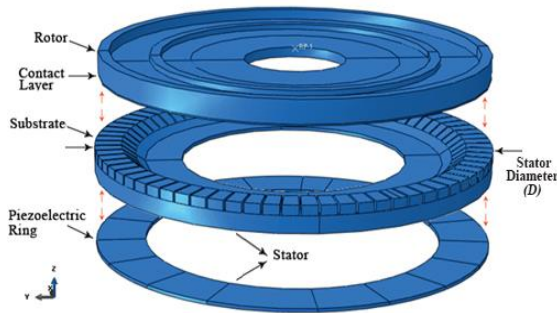


Figure 2. Explosive map of a Mock-Shinsei motor

TABLE 1. Material properties of phosphor bronze [13]

Property	Value
Young's modulus (GPa)	103.5
Poisson's ratio	0.33
Mechanical quality factor (at 0.1 vrms)	3500
Density (Kg/m <sup>3</sup> )	8964

TABLE 2. Material properties of PZT-4 [13, 18]

Property	Value	
Elastic stiffness coefficient (GPa)	$c_{11}^E$	139
	$c_{33}^E$	115
	$c_{44}^E$	25.6
	$c_{66}^E$	30.6
	$c_{12}^E$	77.8
	$c_{13}^E$	74.3
Piezoelectric strain coefficient (C2/m)	$e_{31}$	-5.2
	$e_{15}$	12.7
	$e_{33}$	15.1
Permittivity (nf/m)	$\epsilon_{11}^S$	13.06
	$\epsilon_{33}^S$	11.51
Mechanical quality factor (at 0.01 vrms)	580	
Density (Kg/m <sup>3</sup> )	8560	

TABLE 3. Material Properties of Ekonol/PTFE blend [13, 18]

Property	Value
Elongation storage modulus, E'(GPa)	0.7
Elongation loss modulus, E''(GPa)	0.07
Shear storage modulus, G'(GPa)	0.26
Shear loss modulus, G''(GPa)	0.033
Density (Kg/m <sup>3</sup> )	1950
Coefficient of friction on phosphor bronze	0.3

TABLE 4. Material properties of aluminum [13]

Property	Value
Young's modulus (GPa)	69
Poisson's ratio	0.33
Mechanical quality factor(at 0.1 vrms)	2000
Density (Kg/m <sup>3</sup> )	2720

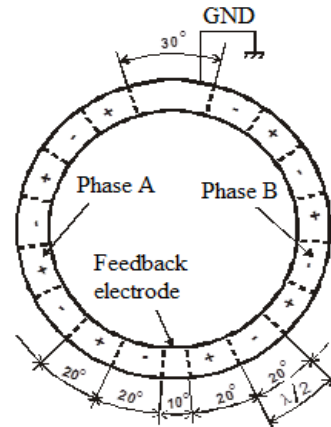


Figure 3. Polarization arrangement of the piezoelectric ring

One of them is assigned to the 8 sectors, as displayed in Figure 4-a, and the other is assigned to the 8 other sectors, according to Figure 4-b. Because the electrical voltage is not applied to the neutral sectors (with 10°, 30° angles), the orientation direction for these sectors is not important and an arbitrary coordinates is assigned to them, as depicted in Figure 4-c. The C3D20RE and C3D20R elements are used for discretizing the piezoelectric ring and other parts, correspondingly.

The length of every two sectors with 20° angle is equal to a wavelength,  $\lambda$ , as shown in Figures 3 and 5. Sector A is shifted three-quarters of wave length out of sector B, according to Figure 3.

When two out-phase high frequency voltage 90° are separately and simultaneously applied to the sectors A and B, the standing waves, generated by these two

voltages are mutually interfered. Figure 5 describes the results in a traveling wave at the surface of the stator with nine wavelengths on the stator. The nine circumferential waves are generated, hence, the mode of standing waves and consequently the travelling-waves will be (9, 0) mode.

**4. NATURAL FREQUENCIES OF THE MOCK-SHINSEI MOTOR**

The Mock-Shinsei motor utilizes the (9, 0) vibration mode. The natural frequencies of (n, o) modes of the stator in the assembled motor are slightly different from those for the free stator, and are equal to the natural frequencies of (n, o) modes of the whole motor. For validation of the model, the natural frequencies of (9, 0) modes of free stator and rotor are obtained, using the Lanczos eigen solution method. Then, the results are compared with the results of [13] which are listed in Table 5. According to this Table, comparison of the results shows good adaptation. Also, Tables 6 and 7 indicate the convergence of the numerical results of the frequencies, regarding the five different meshing groups. Additionally, Figure 6 reveals the convergence curve for the free stator, rotor, and the whole motor.

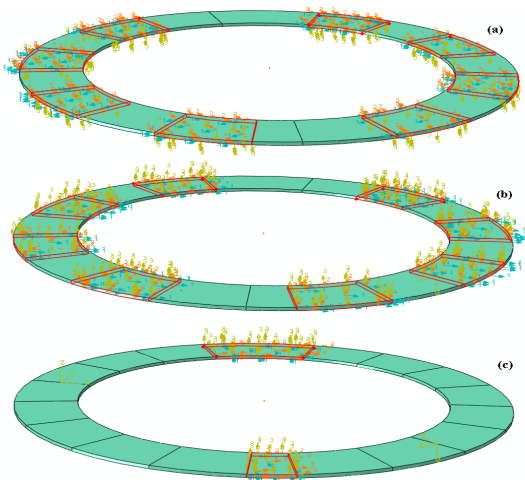


**Figure 4.** Polarization of the piezoelectric ring in the numerical simulations

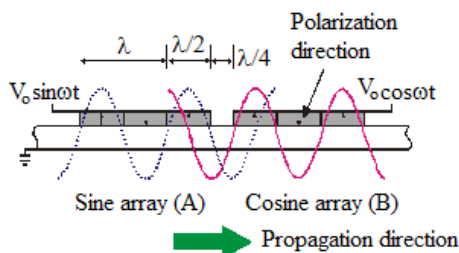


**Figure 5.** Creating the travelling wave in the stator

Since, "mesh 3" is located on the convergence domain (straight horizontal line), it is selected for behavior analysis of the motor in order to reduce time of the simulations and also obtaining the results with acceptable precision.

**5. BEHAVIOUR ANALYSIS OF THE MOCK-SHINSEI MOTOR**

The behavior analysis of the motor needs three steps. The "initial" step is used to apply boundary conditions on the rotor and stator to fix the inner ring of the stator in all directions and the reference point of the rotor in the axial direction of the motor.

**TABLE 5.** Comparison of the frequencies of the Mock-Shinsei motor with the results of Ref. [13]

Natural Frequencies of (9,0) Mode (Hz)			Difference of numerical results with	
Numerical results	Experimental results [13]	FEM results [13]	Experimental results [13]	FEM results [13]
38693	40031	39724	3.3 %	2.6 %
51767	-----	53049	-----	2.4 %
41722	-----	-----	-----	-----

**TABLE 6.** Number of the elements for each mesh group

Part	Mesh 1	Mesh 2	Mesh 3	Mesh 4	Mesh 5
Substrate	1772	2288	4900	6508	8768
Piezo ring	207	352	870	1141	1424
Stator	1979	2640	5770	7649	10192
Rotor	738	960	1834	2403	3000
Motor	2717	3600	7604	10052	13192

**TABLE 7.** Frequencies [Hz] of the Mock-Shinsei motor for each mesh group

Mesh 5	Mesh 4	Mesh 3	Mesh 2	Mesh 1	Part
38631	38693	38693	38666	38597	Stator
51740	51744	51767	51931	52082	Rotor
41649	41708	41727	41528	43812	Motor

**TABLE 8.** Comparison between the stall torque of numerical results and real motor [13]

Numerical results	Real motor [13]	Difference between the numerical and experimental results
0.57	0.55	3.6%

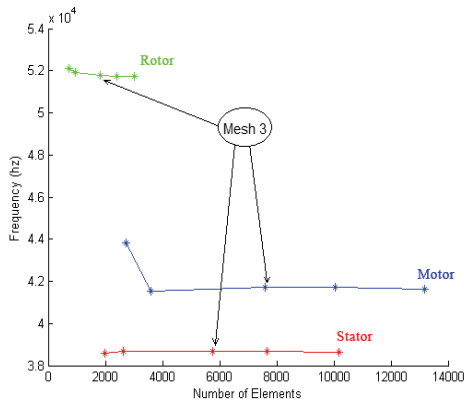


Figure 6. Convergence domain

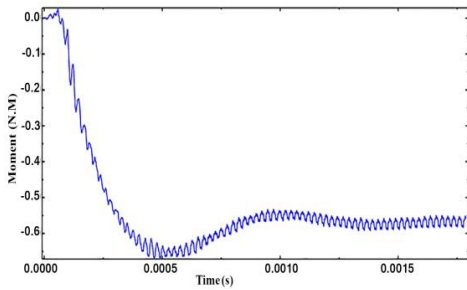


Figure 7. Torque curve of Mock-Shinsei motor,  $RM_3$

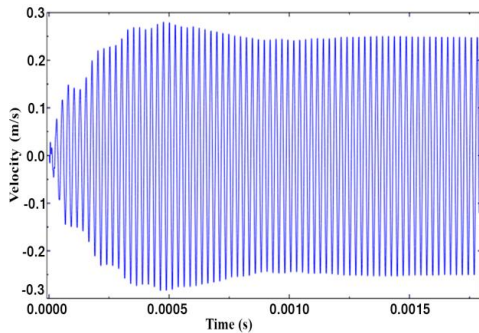


Figure 8. Speed of a point on the middle of stator surface for the Mock-Shinsei,  $V_2$

The next step is utilized "Static, General" to pressing the rotor on the stator by a 160N preload. Finally, "Implicit Dynamic" step is employed to applying two electrical voltages 90° outphase with 150Vp and 40600 Hz to the piezoelectric ring and creating the travelling wave. The analysis is carried out two times. First, the rotation of rotor is fixed in the axial direction of motor and the stall torque,  $RM_3$ , of the motor is calculated in 0.002s, according to Figure 7. Second, the rotation of the rotor in the axial direction is made free (no-load modeling) and the speed of a point on the middle of stator surface,  $V_2$ , is calculated, as shown in Figure 8.

The maximum rotational speed of the rotor,  $\omega_{rotor, no-load}$ , occurs in the no-load condition. Assuming no slipping in the no-load condition, the contact points of the rotor and stator have the same velocity. Hence, the rotational velocity can be considered as [3]:

$$\omega_{rotor, no-load} = V_2 / r_{medium} \tag{4}$$

in which,  $r_{medium}$  is the distance from the center to the middle of contact layer and is equal to 0.0258m. As Figures 7 and 8 reveal, steady state occurs after 0.0015s. Applying the method of averaging, in the steady state,  $RM_3$  and  $V_2$  are obtained as 0.6N.m, 0.25m/s, respectively. Therefore, from Equation (4),  $\omega_{rotor, no-load}$  is approximately equal to 9.7 rad/s.

Table 8, expresses comparison between the stall torque of numerical results and real motor [13]. It illustrates that the difference between stall torque of numerical simulation of Mock-Shinsei motor and real motor is less than 4%, and the numerical simulations has acceptable precision.

## 6. BEHAVIOUR ANALYSIS OF ENLARGED MOCK-SHINSEI MOTOR

From Equation (1), it is expected that duplicating the diameter will increase the stall torque up to 8 times. On the other hand, duplicating the diameter will decrease the resonance frequencies below the ultrasonic rang. The diameter of the motor is doubled to produce larger torque and simultaneously, all thicknesses of the motor are doubled to maintain the resonance frequency in the ultrasonic range. The new motor is named as "enlarged Mock-Shinsei" motor and again is numerically simulated to analyze its behavior.

The (9, 0) mode shape for the enlarged Mock-Shinsei motor is shown in Figure 9. The frequency of this mode shape is equal to 21955 Hz (in the limit of ultrasonic range). To analyze the behavior of the motor, the electrical voltages 90° out phase with 150Vp and 21378 Hz are applied to the piezoelectric sectors and the results are obtained, according to Figures 10 and 11. These figures reveal that the steady state occurs after 0.002s. Employing the method of averaging, in the steady state,  $RM_3$ ,  $V_2$  respectively are 2.4N.m and 0.125 m/s. Moreover, assigning the magnitude of 0.0569m to the  $r_{medium}$  parameter in Equation (4),  $\omega_{rotor, no-load}$  is calculated as 2.2 rad/s.

The numerical results of the behavior analysis of enlarged Mock-Shinsei motor reveals that by duplicating the dimensions of the motor,  $\omega_f$ ,  $\omega_{no-load}$ , and  $T_{Stall}$  will be respectively changed from 40600 Hz to 21378 Hz, 9.7 rad/s to 2.2 rad/s, and 0.57N.m to 2.4 N.m. It confirms that the stall torque of enlarged Mock-Shinsei motor is 4.2 times of the stall torque of the

origin motor. On the other hand, by considering Equations (1-3), it is expected that:

$$T_{Stall} \propto D^3 \omega_f \tag{5}$$

$$T_{Stall(Ent)} = 4.2 * T_{Stall(Orig)} \tag{6}$$

Table 9, indicates the precision of the numerical simulations, compared with the result of Equation (5). Furthermore, it indicates that the numerical simulation stall torque of enlarged Mock-Shinsei motor has less than 5% difference in comparison with the analytical results. Additionally, duplicating the dimensions of Mock-Shinsei motor reveals the following results:

- In comparison with the origin Mock- Shinsei motor, the stall torque of enlarged Mock-Shinsei motor increases 340 percent.
- The maximum rotational speed of enlarged Mock-Shinsei motor decreases 77 percent, when compared to the origin Mock-Shinsei motor.

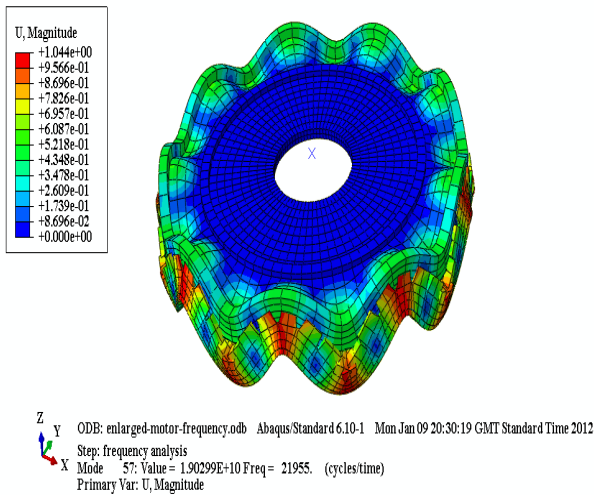


Figure 9. (9, 0) Mode shape of enlarged Mock-Shinsei motor

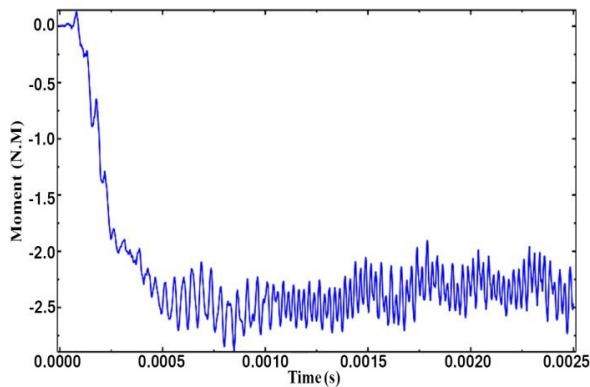


Figure 10. Torque curve of enlarged Mock-Shinsei motor

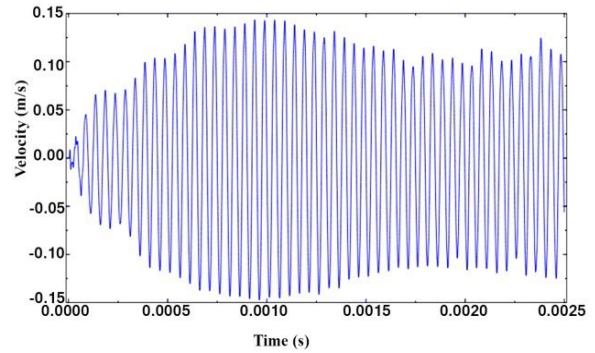


Figure 11. Speed of a point on the middle of stator surface for the enlarged Mock-Shinsei motor,  $V_2$

TABLE 9. Comparison between model of enlarged Mock-Shinsei motor and Equation (5)

Numerical stall torque	Stall torque from Equation 5	Difference
2.4	2.3	4.3%

## 7. CONCLUSIONS

In this paper, first, the USM was numerically simulated; its output torque and rotational speed were achieved and validated. Then, all dimensions of the primary motor were duplicated and again the output torque and rotational speed were obtained. The results of the duplicated motor were validated, applying the theoretical method. The results revealed that increasing the diameter of the USM, will dramatically grow the output torque. On the other hand, increasing USM diameter will reduce the resonance frequency bellow the ultrasonic range and some of this reduction should be compensated by increasing the thickness of the motor.

## 8. REFERENCE

1. Kenjo, T. and Sashida, T., "An introduction to ultrasonic motors, Clarendon Press, (1993).
2. Ikeda, T., "Fundamentals of piezoelectricity", Oxford university press, (1996).
3. Flynn, A. M., "Piezoelectric ultrasonic micromotors", MIT Artificial Intelligence Laboratory, (1995).
4. Uchino, K., "Piezoelectric ultrasonic motors: Overview", *Smart Materials and Structures*, Vol. 7, No. 3, (1998), 273-285.
5. Wallaschek, J., "Contact mechanics of piezoelectric ultrasonic motors", *Smart Materials and Structures*, Vol. 7, No. 3, (1998), 369-381.
6. Hagood IV, N. W. and McFarland, A. J., "Modeling of a piezoelectric rotary ultrasonic motor", *Ultrasonics, Ferroelectrics, and Frequency Control, IEEE Transactions on*, Vol. 42, No. 2, (1995), 210-224.
7. Pons, J., Rodriguez, H., Seco, F., Ceres, R. and Calderon, L., "Modelling of piezoelectric transducers applied to piezoelectric

- motors: A comparative study and new perspective", *Sensors and Actuators A: Physical*, Vol. 110, No. 1, (2004), 336-343.
8. Zhu, M., "Contact analysis and mathematical modeling of traveling wave ultrasonic motors", *Ultrasonics, Ferroelectrics, and Frequency Control, IEEE Transactions on*, Vol. 51, No. 6, (2004), 668-679.
  9. Yerganian, S. S., "Characterization of the damping of a free vibrating piezoelectric motor stator by displacement measurements". Kansas City Plant (KCP), MO, (1999).
  10. el Ghouti, N., "Hybrid modeling of a traveling wave piezoelectric motor, Department of Control Engineering, Aalborg University, (2000).
  11. Mojallali, H., Amini, R., Izadi-Zamanabadi, R. and Jalali, A. A., "Systematic experimental based modeling of a rotary piezoelectric ultrasonic motor", *ISA Transactions*, Vol. 46, No. 1, (2007), 31-40.
  12. Sun, D., Liu, J. and Ai, X., "Modeling and performance evaluation of traveling-wave piezoelectric ultrasonic motors with analytical method", *Sensors and Actuators A: Physical*, Vol. 100, No. 1, (2002), 84-93.
  13. Glenn, T. S., "Mixed-domain performance model of the piezoelectric traveling-wave motor and the development of a two-sided device", Massachusetts Institute of Technology, (2002).
  14. Kim, Y. H. and Ha, S. K., "Analysis of a disk-type stator for the piezoelectric ultrasonic motor using impedance matrix", *Journal of Sound and Vibration*, Vol. 263, No. 3, (2003), 643-663.
  15. Kim, Y. H. and Ha, S. K., "Analysis of a disk-type piezoelectric ultrasonic motor using impedance matrices", *Ultrasonics, Ferroelectrics, and Frequency Control, IEEE Transactions on*, Vol. 50, No. 12, (2003), 1667-1677.
  16. Frangi, A., Corigliano, A., Binci, M. and Faure, P., "Finite element modelling of a rotating piezoelectric ultrasonic motor", *Ultrasonics*, Vol. 43, No. 9, (2005), 747-755.
  17. Chen, Y., Liu, Q. and Zhou, T., "A traveling wave ultrasonic motor of high torque", *Ultrasonics*, Vol. 44, (2006), e581-e584.
  18. Duan, W., Quek, S. T. and Lim, S., "Finite element solution for intermittent-contact problem with piezoelectric actuation in ring type usm", *Finite Elements in Analysis and Design*, Vol. 43, No. 3, (2007), 193-205.
  19. Boumous, Z., Belkhiat, S. and Kebbab, F., "Effect of shearing deformation on the transient response of a traveling wave ultrasonic motor", *Sensors and Actuators A: Physical*, Vol. 150, No. 2, (2009), 243-250.
  20. Duan, W., Quek, S. T. and Wang, Q., "A novel ring type ultrasonic motor with multiple wavenumbers: Design, fabrication and characterization", *Smart Materials and Structures*, Vol. 18, No. 12, (2009), 135-144.
  21. Behzad, M. and Asayesh, M., "Vibration analysis of rotating shaft with loose disk", *International Journal of Engineering Transaction B: Applications*, Vol. 15, No. 4, (2002), 385-393.
  22. Gayathri, M. N., Himavathi, S. and Sankaran, R., "Comparison of MRAS based rotor resistance estimator using reactive power and flux based techniques for space vector pwm inverter fed induction motor drives", *International Journal of Engineering*, Vol. 25, No. 3, (2012), 205-212.
  23. Shah-Mohammadi-Azar, A., Khanchehgardan, A., Rezazadeh, G. and Shabani, R., "Mechanical response of a piezoelectrically sandwiched nano-beam based on the nonlocal theory", *International Journal of Engineering*, Vol. 26, No. 12, (2013), 1515-1524.
  24. Abbasnejad, B., Shabani, R. and Rezazadeh, G., "Stability analysis in parametrically excited electrostatic torsional micro-actuators", *International Journal of Engineering-Transactions C: Aspects*, Vol. 27, No. 3, (2013), 487-498.

## Numerical Prediction of Stator Diameter Effect on the Output Torque of Ultrasonic Traveling-wave Motor, using Finite Elements Simulation

H. Rahafrouz<sup>a</sup>, A. Manouchehrifar<sup>a</sup>, F. Haji Aboutalebi<sup>b</sup>

<sup>a</sup> Department of Mechanical Engineering, Islamic Azad University of Khomeinishahr, Isfahan, Iran

<sup>b</sup> Department of Mechanical Engineering, University of Isfahan, Isfahan, Iran

### PAPER INFO

چکیده

#### Paper history:

Received 29 April 2015

Received in revised form 18 November 2015

Accepted 1 May 2016

#### Keywords:

Ultrasonic Traveling-wave Motor

Increasing the Diameter

Output Torque

Rotational Speed

امروزه مواد پیزوالکتریک کاربرد وسیعی در صنایع مختلف دارند. بنابراین بررسی این مواد و کاربردهای آن از اهمیت ویژه‌ای برخوردار است. در این مقاله، ابتدا فرکانس‌های طبیعی یک موتور پیزوالکتریک موج متحرک با استفاده از شبیه‌سازی‌های اجزاء محدود حاصل می‌شود. سپس، با اعمال ولتاژ الکتریکی متناوب به حلقه پیزوالکتریک، یک موج متحرک در استاتور تولید گردیده و پایداری، اثرات میرایی و خصوصیات موج متحرک مطالعه می‌شود. به علاوه، گشتاور خروجی و سرعت چرخشی موتور محاسبه گردیده و توسط مقادیر عملی اعتبارسنجی می‌شوند. در پایان، قطر استاتور اضافه گردیده و اثرات آن بر روی گشتاور خروجی و سرعت چرخشی بررسی می‌شود. نتایج آشکار می‌کند که گشتاور خروجی و حداکثر سرعت چرخشی موتور بزرگ شده به ترتیب افزایش و کاهش می‌یابد.

doi: 10.5829/idosi.ije.2016.29.05b.16